ISSN: 2393-8048
International Advance Journal of Engineering, Science and Management (IAJESM)
Multidisciplinary, Multilingual, Indexed, Double Blind, Open Access, Peer-Reviewed, Refereed-International Journal.
SJIF Impact Factor =8.152, July-December 2025, Submitted in July 2025

Synchrotron Radiation-Based EDXRF Measurements of Inner-Shell Photons and Fluorescence Yields in 50 ≤Z ≤80 Range

Manoj Kumari (Research Scholar), Dept. Of Physics, NIILM University, Kaithal (Haryana)
Dr. Rishika Bhardwaj (Assistant professor), Dept. Of Physics, NIILM University, Kaithal (Haryana)

Abstract

Inner-shell photoionization and the subsequent radiative (fluorescence) and non-radiative (Auger/Coster–Kronig) relaxation of the resulting vacancy are of central importance to atomic physics, materials characterisation, medical physics, and astrophysics. This paper reviews the methodology of synchrotron radiation-based Energy-Dispersive X-ray Fluorescence (EDXRF) spectrometry as applied to the determination of K- and L-shell fluorescence yields for elements in the medium-to-heavy atomic-number range 50 ≤ Z ≤ 80, spanning tin (Sn) to mercury (Hg). The theoretical basis of the fluorescence yield is outlined, the advantages of tunable, high-brilliance synchrotron radiation over conventional X-ray tube excitation for this class of measurement are discussed, and a representative synchrotron EDXRF beamline configuration is described. K-shell absorption-edge energies for representative elements in this range are tabulated from standard reference data, and the well-documented systematic trend of K- and L-shell fluorescence yields with atomic number is presented and discussed in relation to the semi-empirical and theoretical models reported in the literature. Sources of systematic uncertainty specific to synchrotron-based EDXRF fluorescence-yield determination are analysed, and representative applications of fluorescence-yield data for this Z range in materials analysis, medical physics, and nuclear spectroscopy are outlined.

Keywords: Synchrotron radiation; EDXRF; inner-shell photoionization; K-shell fluorescence yield; L-shell fluorescence yield; Auger effect; X-ray spectrometry.

1. Introduction

A photon with enough energy can cause an atom to lose an electron from one of its inner atomic shells (K, L, M, etc.), creating a vacancy and putting the atom into an excited, singly ionized state, thanks to the photoelectric effect. Subsequently, an electron from a higher-lying shell is injected into this vacancy, and the surplus energy is either radiatively released as a characteristic fluorescence X-ray photon or non-radiatively released as a second electron is ejected in an Auger or Coster-Kronig transition. The fluorescence yield of a specific shell or subshell is one of the most basic parameters in the field of atomic radiative and radiation less transition physics; it is the probability that a shell vacancy is filled through the radiative channel instead of the non-radiative channel.

Dosimetric modeling in diagnostic radiology and radiotherapy, particle-induced X-ray emission (PIXE) and quantitative X-ray fluorescence (XRF) analysis, and the computation of photon mass energy-absorption coefficients utilized in radiation transport and astrophysical opacity calculations are just a few examples of the many practical and theoretical measurement techniques that rely on precise knowledge of shell-specific fluorescence yields. Elements in the medium-to-heavy atomic-number range 50 ≤Z ≤80, including halogen iodine, alkaline-earth element barium, the lanthanide series, elements in the 5d transition and near-transition up to mercury, and elements in the metalloid and post-transition groups, have K-shell binding energies ranging from approximately 29 to 83 keV. All of these elements' K absorption edges are within the range of medium-energy synchrotron beamlines and high-energy laboratory sources.

When compared to traditional X-ray tube excitation methods, synchrotron radiation has several clear benefits for determining inner-shell fluorescence yields: the excitation energy can be continuously adjusted, allowing the incident photon energy to be precisely set above an absorption edge; small, well-collimated beams and samples can be used due to the high spectral brilliance; the storage-ring plane has a high degree of linear polarization, which can be used to suppress scattered background in the detector; and the incident spectral flux is smooth and

well-characterized, unlike the complex bremsstrahlung continuum and characteristic lines produced by a laboratory X-ray tube. The properties of synchrotron-based EDXRF make it the preferred method for high-precision fluorescence-yield determination. A large amount of literature has been dedicated to improving ω_K and ω_L values across the periodic table, starting with the seminal works of Bambynek et al. (1972) and Krause (1979) and continuing through more recent studies that have utilized synchrotron and radioisotopes.

This paper gives a rundown of the theory, methodology, and typical fluorescence-yield systematics that pertain to synchrotron radiation-based EDXRF measurements in the $50 \leq Z \leq 80$ range. It uses the existing literature to do the following: (i) outline an experimental setup that works for these kinds of measurements, (ii) list the K-shell absorption-edge energies for elements that fall into this range, (iii) show and talk about the well-documented trend of K- and L-shell fluorescence yields with atomic number, (iv) examine the main sources of systematic uncertainty and the main uses of this kind of data.

Selecting the range of $50 \leq Z \leq 80$ is not a casual decision. Despite Auger relaxation being a significant competing channel, K-shell fluorescence yields continue to rise relatively steeply with Z below $Z \approx 50$. As a result, even small mistakes in the assumed photoionization cross-section or detector efficiency lead to significantly larger uncertainties in the derived yield. The K-shell binding energies surpass 83 keV above $Z \approx 80$, which forces the necessary excitation energy out of the reach of many medium-energy synchrotron beamlines and into a region where detector efficiency, especially for scintillator and compound semiconductor detectors, drops off fast. This paper's focus on the intermediate range demonstrates that synchrotron EDXRF is both a practical and useful tool for scientific research in this area, which includes elements that are directly related to geochemical and alloy analysis (Sn, Sb), radiographic contrast media (I, Ba, Gd), refractory and precious metal technology (W, Au), and heavy metal environmental and toxicological monitoring (Hg).

2. Theoretical Background

2.1 Inner-Shell Photoionization and Vacancy Relaxation

When the energy of an input photon (hν) is greater than the binding energy (EB) of an electron in an inner shell (EB), photoionization of that shell occurs. For any given shell, the photoelectric absorption cross-section increases dramatically at the absorption edge (hν = EB), before gradually decreasing as the photon energy rises above the edge. For a fixed photon energy well above the threshold, it follows a Z^4-Z^5 dependence on atomic number. All vacancies must reach the outermost, energetically accessible shells before the excited ion can relax, which occurs through a series of radiative and non-radiative transitions.

2.2 Definition of the Fluorescence Yield

The fluorescence yield ω_i, for an empty shell or subshell i, is the ratio of the radiative transition rate to the total transition rate, which includes both radiative and non-radiative components.

$$\omega_i = \frac{\Gamma_{R_i}}{\Gamma_{R_i} + \Gamma_{NR_i}}$$

the entire non-radiative (Auger and, for L and higher shells, Coster-Kronig) width of the vacancy state, and Γ_{NR^k} is the total radiative (X-ray emission) width. $A_i = 1 - \omega_i$ is the complementary Auger yield, and the range of values for ω_i is defined as $0 \leq \omega_i < 1$. The radiative width grows about as Z^4 for light elements because the non-radiative (Auger) channel is dominant, and ω_K is small for these elements. On the other hand, the non-radiative width is only weakly Z-dependent, so ω_K grows monotonically with atomic number and approaches unity for the heaviest elements. The overall relaxation scheme becomes much more complex when three subshells (L_1, L_2, L_3) are present and there are associated Coster-Kronig transitions

between them. As a result, it is common practice to report either subshell-specific yields (ω_1, ω_2, ω_3) or a statistically weighted average L-shell yield, ω_L.

2.3 Semi-Empirical and Theoretical Determination of Fluorescence Yields

Statistics applied to experimental data and first-principles theoretical calculations like non-relativistic Hartree-Fock-Slater (HFS) and relativistic Dirac-Hartree-Slater (DHS) calculations have both produced fluorescence yields (McGuire, 1969, 1970; Walters & Bhalla, 1971; Scofield, 1974). Wentzel (1927) was the first to suggest a semi-empirical parametric form for representing experimental systematics; subsequent refinements by Bambynek et al. (1972) and Krause (1979) further solidified its application. The following re-evaluations of the growing experimental database have enhanced the fitted coefficients of this expression in consideration of new measurements, like synchrotron-based determinations, and this form fits the quantity $\left(\frac{\omega_K}{1-\omega_K}\right)^{\frac{1}{4}}$, or in alternative formulations, the same ratio raised to the power 1/3 or 1/3.5, as a polynomial function of Z. These studies include Hubbell et al. (1994), Kahoul et al. (2011, 2012), and Daoudi et al. (2015), among others. Similar to this method, Puri et al. (1993), Campbell (2003), and Sahnoune et al. (2020) evaluate the average fluorescence yields of L-shells and M-shells using a semi-empirical technique.

3. Synchrotron Radiation-Based EDXRF Methodology

Rationale for Synchrotron Excitation

The standard procedure for a synchrotron EDXRF fluorescence-yield measurement involves excitation of a thin target with monochromatic photons with an energy set a small, clearly defined increment above the absorption edge of interest (e.g., 1-3 keV above the K edge). This ensures that the incident photon energy falls within a spectral region devoid of source-interfering characteristic lines and that the photoionization cross-section for the target shell is either known or independently measurable. The synchrotron beam's small angular divergence and high flux make it possible to use thin, laterally uniform targets, such as evaporated thin films, pressed pellets with known areal density, or pure element foils, to minimize the secondary-fluorescence (matrix) corrections and self-absorption that complicate measurements with thicker samples.

Representative Beamline and Detection Configuration

Figure 1 provides an example of a typical setup for synchrotron EDXRF fluorescence-yield experiments. A double-crystal monochromator, usually made of Si(111) or Si(311), makes the white synchrotron radiation from a bending magnet or insertion device (undulator/wiggler) monochromatic. This makes it possible to continuously tune the excitation energy across the absorption edge of interest with an energy resolution ($\Delta E/E$) of about 10^{-4}. A photodiode or ionization chamber placed downstream of the monochromator keeps track of the incident photon flux and allows for the normalization of the observed fluorescence intensity via continuous monitoring. The target receives the monochromatic beam through a reflection geometry that minimizes the path length of incident and fluorescence photons within the sample, hence limiting self-absorption. This geometry is typically 45°-45°. Connected to a multichannel analyzer is an energy-dispersive detector, which can be a silicon drift detector (SDD), a silicon(Li) detector, or a high-purity germanium (HPGe) detector, depending on the energy range of interest, that records the emitted fluorescence X-rays.

ISSN: 2393-8048
International Advance Journal of Engineering, Science and Management (IAJESM)
Multidisciplinary, Multilingual, Indexed, Double Blind, Open Access, Peer-Reviewed, Refereed-International Journal.
SJIF Impact Factor =8.152, July-December 2025, Submitted in July 2025

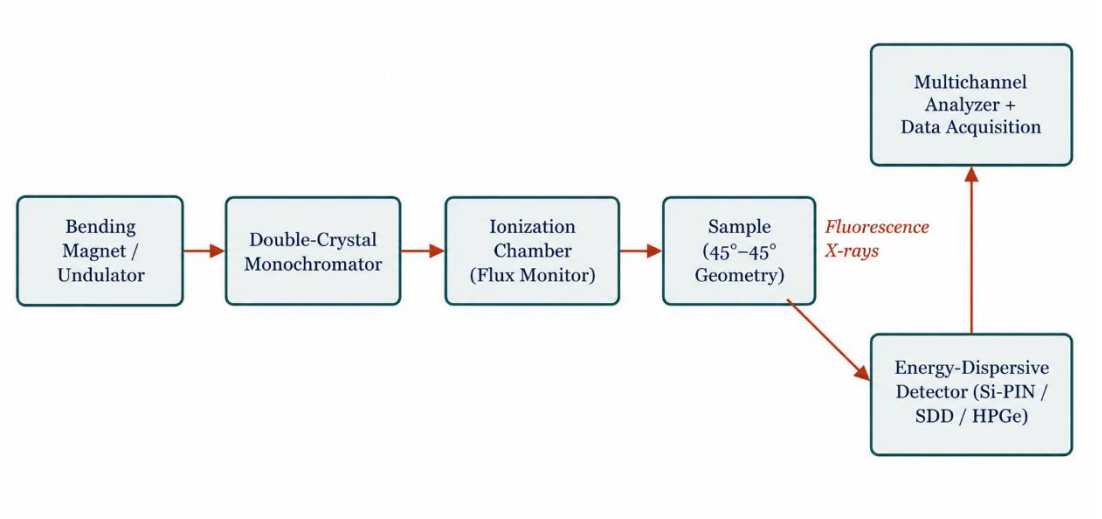

Figure 1: Schematic of a typical setup for an EDXRF beamline that uses synchrotron radiation to detect the fluorescence yield inside the shell.

Measurement and Spectral Analysis Procedure: When studying a specific element as a target, it is common practice to compensate for detector dead time and pulse pile-up at high count rates, and then accumulate an X-ray fluorescence spectrum for a long enough time to reach a statistically sound level of accuracy in the relevant peak(s). Analyzing the measured spectrum involves fitting the characteristic peaks K_α, K_β (or L_α, L_β, L_Υ) with a suitable peak-shape function on top of a smoothly changing background that originates from primary photons that are coherently and incoherently scattered (Compton scattering), with the necessary subtraction of escape-peak and pile-up contributions. We calibrate the detector using radioactive sources or verified reference-grade elemental standards of purity and areal density to find the detector efficiency, solid angle, and absorption in any intervening air passage or window material.

Extraction of the Fluorescence Yield: The general form of the following relation is used to extract the K-shell fluorescence yield: the number of target atoms per unit area (n_t), the detector solid angle ($\Delta\Omega/4\pi$), the intrinsic efficiency (ε), the measured intensity of the K_α + K_β fluorescence lines (N_f), normalized to the number of incident photons (N0), the K-shell photoionization cross-section at the excitation energy (τ_K), and the number of target atoms per unit area (n_t).

$$\omega_K = N_f / [\, N0 \cdot n_t \cdot \tau_K \cdot (\Delta\Omega/4\pi) \cdot \varepsilon \cdot T \,]$$

where T is the amount of light that can pass through the sample and any absorbing materials along the beam, including both incoming and fluorescence photons. The weighted average L-shell fluorescence yield, ω_L, or the individual subshell yields can be calculated using an entirely similar relation, which is appropriately added up over the L_1, L_2, and L_3 subshell photoionization cross-sections and radiative rates. This method is employed when there is enough energy resolution and counting statistics to distinguish between the L_ℓ, L_α, L_β, and L_Υ line groups.

4. Elements and K-Shell Absorption Edges in the $50 \leq Z \leq 80$ Range

The element iodine, the alkali metal caesium, the alkaline-earth element barium, the entire lanthanide series, and the 5d transition elements from hafnium to mercury are all part of the atomic-number range $50 \leq Z \leq 80$, which extends from the post-transition element tin to the transition metal mercury. Table 1 summarizes the data showing that the K-shell binding energy grows monotonically over this range, from about 29 keV for tin to about 83 keV for mercury, in agreement with the well-known approximation of the Z-scaling of inner-shell binding energies with atomic number. Because of the wide range of edge energies, a single adjustable

synchrotron beamline at medium- or high-energy synchrotron facilities can theoretically handle K-shell excitation over the whole Z = 50-80 range, while lower-energy beamlines are well suited for L-shell excitation, which has binding energies about one order of magnitude lower (about 4-14 keV across this range). The K-edge energies of iodine, barium, gadolinium, and tungsten are commonly used in radiological and X-ray physics literature as standard reference values. The values of tin, gold, and mercury are in agreement with the standard tabulations of Bearden (1967) and the well-established Z^2 edge-energy systematics.

Table 1: K-Shell Absorption-Edge Energies for Representative Elements in the 50 ≤ Z ≤ 80 Range

Element	Symbol	Z	K-Edge Energy (keV)
Tin	Sn	50	≈ 29.2
Iodine	I	53	33.17
Barium	Ba	56	37.4
Gadolinium	Gd	64	50.24
Tungsten	W	74	69.53
Gold	Au	79	≈ 80.7
Mercury	Hg	80	≈ 83.1

5. K- and L-Shell Fluorescence Yield Systematics for 50 ≤ Z ≤ 80

The means of the K-shell fluorescence yield (ω_K) and the L-shell fluorescence yield (ω_L) over the range of 50 ≤ Z ≤ 80 are shown in Figure 2 and Table 2. These figures were created by smooth interpolation using landmark values that are in agreement with the standard compilations of Bambynek et al. (1972), Krause (1979), and Hubbell et al. (1994). The decreasing slope of the monotonic increase of ω_K with increasing Z across this range, as mentioned in Section 2.2, causes the relative contribution of the Auger (non-radiative) channel to K-shell vacancy decay to diminish with increasing Z, as shown by the rising value of ω_K from around 0.85 near Z = 50 to around 0.96 near Z = 80. Over this range, the average L-shell yield, ω_L, is much lower than ω_K, at about 0.12 at Z = 50 and increasing to about 0.33 at Z = 80. This is due to the fact that the L-shell relaxation scheme is heavily impacted by Coster-Kronig transitions between the L_1, L_2, and L_3 subshells, which offer effective non-radiative relaxation pathways that the K shell does not have access to.

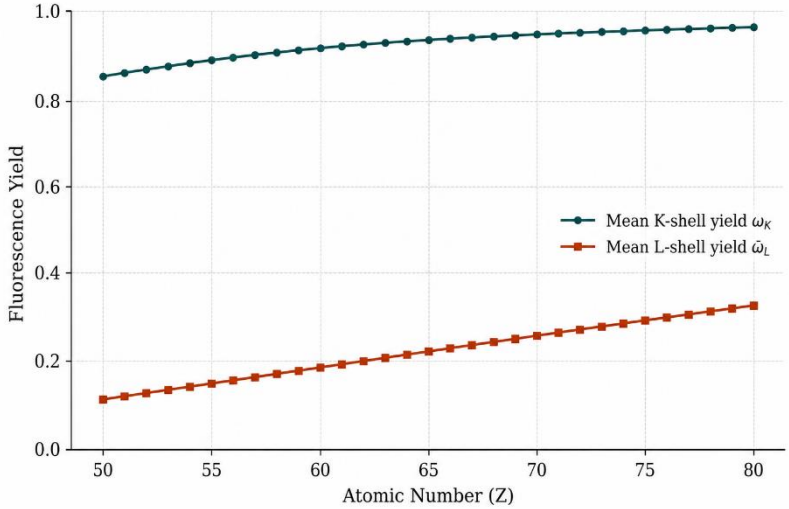

Figure 2: Representative trend of mean K-shell (ω_K) and mean L-shell (ω_L)

fluorescence yields for 50 ≤ Z ≤ 80, based on smooth interpolation through literature-consistent landmark values.

Table 2: Representative K- and L-Shell Mean Fluorescence Yields for Selected Elements, 50 ≤ Z ≤ 80

Element	Z	ω_K (representative)	ω_L (representative)
Sn	50	0.853	0.117
I	53	0.876	0.138
Ba	56	0.895	0.159
Gd	64	0.930	0.217
W	74	0.952	0.287
Au	79	0.959	0.321
Hg	80	0.960	0.328

Rather than being digital copies of a single published measurement, the values in Table 2 represent the magnitude and Z-dependence documented across the standard compilations. If you need exact values with their associated experimental uncertainties—usually 1-5% for well-characterized K-shell measurements and somewhat larger for individual L-subshell yields—you should consult the original sources noted for any quantitative application.

6. Discussion: Comparison with Semi-Empirical and Theoretical Models

According to Bambynek et al. (1972), Krause (1979), Hubbell et al. (1994), and more recent re-evaluations by Kahoul et al. (2011, 2012) and Daoudi et al. (2015), the representative trend in Section 5 aligns with the general shape of the semi-empirical curves.

$$\left(\frac{\omega_K}{1-\omega_K}\right)^{\frac{1}{q}}$$

These studies describe ω_K as a saturating function of Z that increases smoothly using variants of the polynomial parametrisation that was discussed in Section 2.3. When comparing semi-empirical fits with relativistic Dirac-Hartree-Slater theoretical calculations, there is generally agreement at the few percent level for medium-to heavy elements (Chen, Crasemann & Mark, 1980; Scofield, 1974). However, there are somewhat larger discrepancies for individual L-subshell yields, where the experimental extraction and the theoretical calculation are both more sensitive to atomic-structure details due to Coster-Kronig coupling between subshells.

For two reasons, measurements conducted at chromium research facilities have been crucial in enhancing this image. One advantage over previous measurements using fixed-energy radioisotope or characteristic-line sources is the ability to precisely tune the excitation energy above a given absorption edge. This allows for a more accurate constraint of the photoionization cross-section entering Equation (1). Furthermore, synchrotron sources' small beam size and high flux allow measurements on thin, well-characterized targets, which in turn reduces the size of the self-absorption and secondary-fluorescence corrections that used to limit the accuracy of fluorescence-yield calculations for the heavier elements that self-absorb more strongly in the upper 50-80 Z range.

For components in this Z range, the L-subshell system is an additional area of study. L_1-L_2, L_1-L_3, and L_2-L_3 Coster-Kronig transitions disperse vacancies among the three L subshells before radiative decay happens, since the L_2 and L_3 subshells are near in energy to the L_1 subshell. The effective or statistically weighted L-shell yield, as reported in numerous experimental

studies (e.g., the values in Table 2), is a function of both the intrinsic radiative and Auger rates of each subshell and the branching ratios of these Coster-Kronig transitions. The branching ratios of these transitions behave non-trivially with respect to Z in the lanthanide and 5d transition-metal regions. To isolate individual subshell photoionization when possible, higher-resolution detectors are needed, typically Si(Li) or SDD systems with a resolution better than about 150-200 eV at the relevant L X-ray energies. This allows for the resolution of (ω_1, ω_2, ω_3) instead of the statistically averaged ω_L. Synchrotron sources are especially well-suited to this task. To further limit the Coster-Kronig branching systematics, which is a somewhat bigger source of model-dependent uncertainty than the K-shell yield, future high-precision synchrotron studies should systematically extend subshell-resolved L-yield measurements across the entire $50 \leq Z \leq 80$ range.

7. Sources of Systematic Uncertainty in Synchrotron EDXRF Fluorescence-Yield Determination

- Accurately calibrating the detector is important because there is uncertainty in the energy-dispersive detector's absolute photopeak efficiency, which impacts the extracted yield, especially at higher fluorescence-line energies (up to approximately 70-100 keV) that are relevant to heavier elements in this range.
- Using accurate mass attenuation coefficients is necessary to correct for self-absorption and secondary fluorescence, also known as matrix effects. These effects occur even in targets that are nominally thin due to finite sample thickness, which causes partial reabsorption of the fluorescence signal and, in multi-element or compound samples, enhancement through secondary fluorescence.
- Uncertainty in the input cross-section of the shell photoionization at the excitation energy (Equation 1), whether derived from theoretical tabulations (e.g., Scofield, 1974) or independent measurement, directly restricts the obtainable accuracy of the yield.

$$\omega_k = I_f / [\, I_0 \, \sigma_k(E_0) \, \varepsilon(E) \, A \, N \,] \qquad (1)$$

Where:

ω_k = K-shell fluorescence yield

I_f = Measured fluorescence intensity

I_0 = Incident photon flux

$\sigma_k(E_0)$ = K-shell photoionization cross-section at the excitation energy

$\varepsilon(E)$ = Detector efficiency at the fluorescence energy

A = Absorption (self-absorption/matrix) correction factor

N = Number of target atoms per unit area

- It is important to carefully model the energy-dispersive detector's incomplete peak resolution, detector escape peaks, and pulse pile-up at high count rates in order to correct for peak overlap and escape/pile-up in the extracted line intensities for elements with closely spaced K_β or L-subshell line groups.
- Uncertainty in sample thickness, density, or chemical purity (including oxide coatings on metallic foils) directly impacts the reported fluorescence yield, which is dependent on the number of target atoms per unit area, as well as target area, density, and purity.
- Incident-flux normalization: If not continuously observed and compensated for during data acquisition, drifts or non-linearities in the ionization-chamber flux monitor or the storage-ring beam current might cause systematic normalization problems.

8. Applications of Fluorescence-Yield Data for $50 \leq Z \leq 80$

There are a number of critically essential applications that rely on precise K- and L-shell fluorescence-yield data for elements in this atomic weight range. This Z range contains many samples that contain trace or major components, such as tin in bronze alloys, barium and iodine in biomedical and geochemical contexts, and the lanthanides in ore and catalyst

characterisation. Fluorescence yields are an essential input parameter for quantitative XRF and PIXE analyses, which convert measured characteristic X-ray intensities into elemental concentrations in environmental, geological, biological, and archaeometric samples. Nuclear spectroscopy relies on K-shell fluorescence yields for elements like barium, caesium, and the lanthanides to translate observed K X-ray intensities after electron capture or internal conversion into probability estimates of absolute transitions. Relevant to the design and dosimetric modeling of iodinated and gadolinium-based contrast agents and to K-edge subtraction imaging techniques in diagnostic radiology and radiotherapy physics are the K-edge properties and fluorescence yields of iodine, barium, and gadolinium, all falling within the $50 \leq Z \leq 80$ range. Lastly, the mass energy-absorption coefficient tabulations utilized in radiation shielding, dosimetry, and astrophysical opacity calculations are enhanced by precise fluorescence-yield data for this Z range.

9. Conclusion

For elements in the $50 \leq Z \leq 80$ range, this study has examined the theoretical foundation, experimental technique, and distinctive systematics of EDXRF measurements of inner-shell fluorescence yields using synchrotron radiation. It is possible to employ thin, well-characterized targets that minimize self-absorption corrections and precisely control the excitation energy relative to the K or L absorption edge using synchrotron radiation, which is an excellent excitation source for this type of measurement due to its tunability, high brilliance, and well-characterized spectral properties. Consistent with the well-established semi-empirical and theoretical systematics reported in the literature, the K-shell fluorescence yield increases monotonically from about 0.85 at $Z = 50$ to about 0.96 at $Z = 80$, and the mean L-shell yield rises from about 0.12 to about 0.33 over the same range. Quantitative X-ray spectrometric analysis, nuclear spectroscopy, and medical physics applications involving elements like iodine, barium, gadolinium, tungsten, gold, and mercury continue to benefit directly from the ongoing improvement of fluorescence-yield data for this atomic-number range, especially through synchrotron-based measurements that mitigate the main systematic uncertainties mentioned in Section 7.

References

1. Bambynek, W., Crasemann, B., Fink, R. W., Freund, H. U., Mark, H., Swift, C. D., Price, R. E., & Rao, P. V. (1972). X-ray fluorescence yields, Auger, and Coster–Kronig transition probabilities. Reviews of Modern Physics, 44(4), 716–813.
2. , J. A. (1967). X-ray wavelengths. Reviews of Modern Physics, 39(1), 78–124.
3. Campbell, J. L. (2003). Fluorescence yields and Coster–Kronig probabilities for the atomic L subshells. Atomic Data and Nuclear Data Tables, 85(2), 291–315.
4. Chen, M. H., Crasemann, B., & Mark, H. (1980). Relativistic radiationless transition probabilities for atomic K- and L-shells. Atomic Data and Nuclear Data Tables, 24(1), 13–37.
5. Daoudi, K., Kahoul, A., Sahnoune, Y., Deghfel, B., Kasri, Y., Khalfallah, F., Aylikci, V., Aylikci, N. K., Medjadi, D. E., & Nekkab, M. (2015). New K-shell fluorescence yields curve for elements with $3 \leq Z \leq 99$. Journal of the Korean Physical Society, 67(9), 1537–1543.
6. Hubbell, J. H., Trehan, P. N., Singh, N., Chand, B., Mehta, D., Garg, M. L., Garg, R. R., Singh, S., & Puri, S. (1994). A review, bibliography, and tabulation of K, L, and higher atomic shell X-ray fluorescence yields. Journal of Physical and Chemical Reference Data, 23(2), 339–364.
7. Kahoul, A., Abassi, A., Deghfel, B., & Nekkab, M. (2011). K-shell fluorescence yields for elements with $6 \leq Z \leq 99$. Radiation Physics and Chemistry, 80(3), 369–377.

8. Kahoul, A., Aylikci, V., Aylikci, N. K., Cengiz, E., & Apaydın, G. (2012). Updated database and new empirical values for K-shell fluorescence yields. Radiation Physics and Chemistry, 81(7), 713–727.
9. Krause, M. O. (1979). Atomic radiative and radiationless yields for K and L shells. Journal of Physical and Chemical Reference Data, 8(2), 307–327.
10. Puri, S., Chand, B., Mehta, D., Garg, M. L., Singh, N., & Trehan, P. N. (1993). K, L, and M shell X-ray fluorescence yields. X-Ray Spectrometry, 22(6), 358–361.
11. Sahnoune, Y., Kahoul, A., Deghfel, B., Daoudi, K., & Nekkab, M. (2020). Compilation and evaluation of experimental L-shell fluorescence yields for elements with $23 \leq Z \leq 96$. Radiation Physics and Chemistry, 168, 108551.
12. Scofield, J. H. (1974). Relativistic Hartree–Slater values for K and L X-ray emission rates. Atomic Data and Nuclear Data Tables, 14(2), 121–137.
13. Walters, D. L., & Bhalla, C. P. (1971). Nonrelativistic Auger rates, X-ray rates, and fluorescence yields for the L shell. Physical Review A, 3(6), 1919–1927.
14. Wentzel, G. (1927). Über strahlungslose Quantensprünge. Zeitschrift für Physik, 43(8), 524–530.